



HAL
open science

Bioinjection treatment: Effects of post-injection residual stress on left ventricular wall stress

Lik Chuan Lee, Samuel T. Wall, Martin Genet, Andy Hinson, Julius M. Guccione

► **To cite this version:**

Lik Chuan Lee, Samuel T. Wall, Martin Genet, Andy Hinson, Julius M. Guccione. Bioinjection treatment: Effects of post-injection residual stress on left ventricular wall stress. *Journal of Biomechanics*, 2014, 47 (12), pp.4. 10.1016/j.jbiomech.2014.06.026 . hal-01196372

HAL Id: hal-01196372

<https://hal.science/hal-01196372>

Submitted on 5 Jan 2017

HAL is a multi-disciplinary open access archive for the deposit and dissemination of scientific research documents, whether they are published or not. The documents may come from teaching and research institutions in France or abroad, or from public or private research centers.

L'archive ouverte pluridisciplinaire **HAL**, est destinée au dépôt et à la diffusion de documents scientifiques de niveau recherche, publiés ou non, émanant des établissements d'enseignement et de recherche français ou étrangers, des laboratoires publics ou privés.

1 **BIOINJECTION TREATMENT: EFFECTS OF POST-INJECTION RESIDUAL STRESS**
2 **ON LEFT VENTRICULAR WALL STRESS**

3 **Lik Chuan Lee^{1,2,3}, Samuel T. Wall⁴, Martin Genet^{1,2,3,5}, Andy Hinson⁶ and Julius M.**
4 **Guccione^{1,2,3}**

5 Department of Surgery¹, Bioengineering² and Medicine³ University of California, San
6 Francisco, CA; Simula Research Laboratory⁴, Oslo, Norway; Marie-Curie Outgoing
7 fellow⁵; Lonestar Heart Inc⁶.

8

9

10

11 **Word count: 3729**

12

13

14

15

16

17

18

19

20

21

22

23

24 **Corresponding Author:**

25 Lik Chuan, Lee, PhD

26 Department of Surgery, School of Medicine,

27 University of California, San Francisco,

28 Mount Zion Harold Brunn Institute for Cardiovascular Research,

29 1657 Scott St., Room 219,

30 San Francisco, CA 94143,

31 Phone: +1 (510) 316-2102

32 Email: LikChuan.Lee@ucsfmedctr.org

33

34 **ABSTRACT**

35

36 Injection of biomaterials into diseased myocardium has been associated with decreased myofiber
37 stress, restored left ventricular (LV) geometry and improved LV function. However, its exact
38 mechanism(s) of action remained unclear. In this work, we present the first patient-specific
39 computational model of biomaterial injection that accounts for the possibility of residual strain
40 and stress introduced by this treatment. We show that the presence of residual stress can create
41 more heterogeneous regional myofiber stress and strain fields. Our simulation results show that
42 the treatment generates low stress and stretch areas between injection sites, and high stress and
43 stretch areas between the injections and both the endocardium and epicardium. Globally, these
44 local changes are translated into an increase in average myofiber stress and its standard deviation
45 (from 6.9 ± 4.6 to 11.2 ± 48.8 kPa and 30 ± 15 to 35.1 ± 50.9 kPa at end-diastole and end-
46 systole, respectively). These results suggest that the residual stress and strain possibly generated
47 by biomaterial injection treatment can have large effects on the regional myocardial stress and
48 strain fields, which may be important in the remodeling process.

49

50

51

52 **Keywords:** Congestive heart failure, biomaterial injection, left ventricular wall stress,
53 mathematical modeling, magnetic resonance imaging.

54

55 **1. INTRODUCTION**

56 Injection of materials into the myocardium as a treatment for heart diseases has generated
57 considerable interest over recent years. The injection of biomaterials, which range from
58 biological materials e.g., Alginate (Landa et al., 2008) and Fibrin (Christman et al., 2004), to
59 synthetic hydrogels (Jiang et al., 2009), have shown positive outcomes in animal studies.
60 Recently, significant reverse remodeling – 50% reduction in end-diastolic volume (EDV) and
61 end-systolic volume (ESV) – in patients suffering from dilated cardiomyopathy was observed as
62 early as 3 months after injection of Algiysl-LVR™ (a calcium-sodium alginate hydrogel) and
63 Coronary Artery Bypass Grafting (Lee et al., 2013a).

64
65 Despite these favorable outcomes, the exact mechanism(s) of action of the injection treatment
66 remain(s) unclear. While the treatment’s primary rationale is to provide support to the diseased
67 myocardium to reduce ventricular wall stress (widely believed to be responsible for adverse
68 cardiac remodeling), there are also suggestions that these injected biomaterials can create a
69 “healthier micro-environment through stress shielding” that increases capillary and arteriole
70 densities (Nelson et al., 2011). Thus, the effects of this treatment need to be better understood,
71 especially because of its potential as an effective treatment for heart diseases.

72
73 Computational modeling has been used to better understand the effects of injecting material into
74 the myocardium (Kortsmit et al., 2012; Wall et al., 2006; Wenk et al., 2009). These modeling
75 studies generally support the primary rationale of the injection treatment: helping to provide
76 support to the myocardium through thickening of the ventricular wall to reduce ventricular wall
77 stress. However, these studies did not include the possible effects of residual stress that could
78 occur when injections are introduced into the myocardium.

79
80 Injectable biomaterials usually begin in a viscous liquid that solidifies through chemical changes
81 *in situ* to form a solid hydrogel (Christman et al., 2004; Lee et al., 2013b). When injected, these
82 liquids are forced into the myocardium, creating new space to accommodate the blob of material.
83 As such, residual stress can be introduced during this process, especially when the void that
84 accommodates the injection has an initial volume smaller than the injected volume itself.
85 Although the myocardial extracellular space (~ 24% of the tissue space) consists of about 6%

86 “empty” space devoid of any structural components (Frank and Langer, 1974) - about 2.7 ml for
87 a left ventricular (LV) wall volume of 190 ml in the patient-specific model described here, they
88 are interspersed within the myocardium and the local “empty” space is substantially smaller.
89 Hence, it is likely that residual stress could be present when the injection volume ~ 0.3 ml (Lee
90 et al., 2013a) is greater than the local “empty” or void space.

91

92 The primary aims of this paper are twofold: first, to describe a methodology to model the effects
93 of post-injection residual stress, and second, to highlight the possible effects of residual stress on
94 local myofiber stress and stretch fields.

95

96

97 **2. METHODS AND RESULTS**

98 **2.1 Finite element model of the LV**

99 A patient-specific finite element (FE) model of the LV was constructed based on the baseline
100 magnetic resonance (MR) images of patient 1 described in Lee et al. (2013a). The patient was
101 diagnosed with NYHA class III heart failure and had ischemic cardiomyopathy, hypertension,
102 hyperlipidemia and renal insufficiency. The LV was modeled using 110,976 trilinear hexahedral
103 elements and the FE mesh was graded so that its mesh density was 4 times higher at the mid-LV
104 (where the injections are located) (**Figure 1a**).

105 Nearly incompressible and transversely isotropic hyperelastic material laws for the passive
106 (Guccione et al., 1991) and active myocardium (Guccione et al., 1993) were used to model the
107 mechanical behavior of the LV during a cardiac cycle. The material passive stiffness (C) and the
108 tissue contractility (T_{\max}) were chosen so that the predicted LV volumes (without injection)
109 matched the corresponding EDV (197ml) and ESV (122ml) measured from MR images. All
110 other parameters had values equal to those used in large animal studies (Sun et al., 2009) and
111 human study (Wenk et al., 2012).

112 Local fiber direction was defined on the local tangent plane by prescribing a fiber angle taken
113 with respect to the local circumferential vector running counterclockwise when viewed in the
114 base-to-apex direction. In the entire LV, the fiber angle varied linearly from the endocardium

115 (60°) to the epicardium (-60°) (Streeter et al., 1969) (**Figure 1b**). The epicardial-base edge was
116 fixed, whereas the base displacement was constrained in the out-of-plane direction.

117 Three simulation cases, namely, BASELINE, RESIDUAL and NO-RESIDUAL were performed.
118 BASELINE was defined to be the case before injections. RESIDUAL and NO-RESIDUAL
119 corresponded to the post-injection cases with and without the effects of residual stress,
120 respectively.

121

122 **2.2 Modeling injections into the LV**

123 The LV wall was meshed with spherical voids at the mid LV (halfway between the base and the
124 apex) and the voids were filled with hexahedral elements. The finite element meshes of the voids
125 and the LV wall have matching nodes at their common interface. There were a total of 12 voids,
126 each with an arbitrarily prescribed radius of 1mm (**Figure 1c**).

127 To model the effects arising from post-injection residual stress (RESIDUAL), the hexahedral
128 elements in the void were first prescribed with a dummy material law and a spherical
129 displacement field was then imposed to dilate each void to an arbitrary prescribed injection
130 volume of 0.02 ml. Thereafter, stresses were initialized to zero in the elements defining the void
131 and these elements were prescribed with a material law describing the hydrogel injections. In
132 other words, the elements within the void now define the injected hydrogel. The hydrogel
133 injections were modeled using nearly incompressible Mooney-Rivlin material law with
134 previously obtained parameters (Wenk et al., 2009) from Alginate experiments. Then, the
135 spherical displacement field was removed to allow the injections and the LV to deform until a
136 force-equilibrium was reached (**Figure 1d**). This resultant configuration is defined to be the
137 unloaded (but not stress-free) configuration. In NO-RESIDUAL, stresses of both the injections
138 and LV wall were initialized to zero from the unloaded configuration of the RESIDUAL case.

139 End-diastole (ED) and end-systole (ES) were simulated in all 3 cases by imposing a pressure
140 boundary condition of 20 mm Hg and 125 mm Hg at the endocardial wall in the unloaded
141 configuration, respectively. All simulations were performed using LS-DYNA (Livermore

142 Software Technology Corporation, Livermore, CA) with the passive and active myocardial
143 material law implemented as a user-defined material subroutine.

144

145 **2.3 Effect on Global Stretch and Stress in Myofiber and Cross-myofiber directions.**

146 Stretch and stress in both the myofiber and cross-myofiber directions were averaged over the
147 entire LV at ED and ES for BASELINE, RESIDUAL and NO-RESIDUAL (**Table 1**). The
148 average stress and stretch (at ES and ED) were not very different between BASELINE and NO-
149 RESIDUAL in both the myofiber and cross-myofiber directions. However, the average ED
150 myofiber stress of RESIDUAL (11.2 ± 48.8 kPa) was nearly twice as large as that of BASELINE
151 (6.9 ± 4.6 kPa), whereas the average ES myofiber stress of RESIDUAL (35.1 ± 50.9 kPa) was
152 17% higher than that of BASELINE (30 ± 15 kPa). Similar trend was also observed for the
153 cross-myofiber stress of RESIDUAL, which was higher than BASELINE. The average ED and
154 ES stretch of RESIDUAL was not very different from that of BASELINE in both the myofiber
155 and cross-myofiber directions. In general, both ES and ED stress and stretch in RESIDUAL had
156 larger values of standard deviation than BASELINE and NO-RESIDUAL.

157

158 **2.4 Effect on Local Myofiber Stretch and Stress**

159 The substantially larger standard deviation found in RESIDUAL suggests that the myofiber
160 stress and stretch were more heterogeneous than the other 2 cases. Moreover, the significantly
161 larger change in fiber stress than in fiber stretch indicates that out-of-fiber-direction tensions and
162 shear-stress components must be activated.

163 Closer inspection of the myofiber stretch and stress fields reveals an organized pattern in the
164 injection region, particularly in RESIDUAL when compared to NO-RESIDUAL (**Figures 2 and**
165 **3**). In RESIDUAL, the myofiber stretch was substantially decreased and was less than unity at
166 the mid wall between injections at both ED and ES. At ES, the myofiber stretch was elevated in
167 the transmural direction between the injections and both the endocardium and epicardium. The
168 ES myofiber stress field displayed similar pattern as that of the ES myofiber stretch.
169 Contrastingly, ED myofiber stress did not decrease substantially between injections at the mid

170 wall and was elevated in the transmural direction between the injections and both epicardium and
171 endocardium.

172 Without residual stress (NO-RESIDUAL), the myofiber stretch and stress fields at the injection
173 region were largely similar to those in BASELINE, with the exception that the ED and ES
174 myofiber stress between injections was slightly lower than in BASELINE (**Figure 3**).

175

176 **2.5 Effect of void-to-injection size ratio on myofiber stress**

177 The myofiber stress is also sensitive to the void-to-injection size ratio. By keeping the void size
178 constant, both global ES and ED average myofiber stress decreases with decreasing injection
179 volume (**Figure 4a**). In addition, the standard deviation of the myofiber stress also decreased
180 substantially with decreasing injection volume and approaches the values in NO-RESIDUAL.
181 Correspondingly, the myofiber stress field became more homogeneous near the injection sites
182 (**Figure 4b**).

183

184 **2.6 Effect on ventricular volume**

185 The injections had little effects on both EDV and ESV in RESIDUAL and NO-RESIDUAL.
186 Only in RESIDUAL was the EDV slightly smaller (198 ml) than BASELINE (201ml).

187

188 **3. DISCUSSIONS**

189 **3.1 Myofiber stretch and stress heterogeneity**

190 Although the global averaged myofiber stress became elevated when residual stress due to the
191 injection was present, this increase was associated with a greater increase in its standard
192 deviation. As such, the principal finding of our simulation is the increase in heterogeneity of the
193 myofiber stretch and stress fields when residual stress is present, but not in the overall increase in
194 myofiber stress. Specifically, the presence of residual stress produced a regular pattern of low
195 myofiber stretch between injections in the LV mid wall, and high myofiber stretch extending

196 from the injections towards the endocardium and epicardium (**Figures 2** and **3**). The less than
197 unity myofiber stretch between the injections at ED and ES implies that the midwall myofibers
198 were compressed or “unloaded” throughout the cardiac cycle. This result can be explained by
199 considering the myofiber orientation across the LV wall (**Figure 1b**). Because myofibers are
200 oriented circumferentially at the midwall, they were compressed by the expanding voids that
201 accommodated the injections. Contrastingly, the expanding voids also stretch the obliquely-
202 oriented sub-endocardial and sub-epicardial myofibers.

203 The transmurally elongated ellipsoidal shape of the injection in the unloaded configuration
204 (**Figure 1b**) is a consequence of (a) our assumption of a spherical void and (b) the anisotropic
205 material behavior of the myocardium. Given that the LV wall is stiffest in the myofiber direction
206 in our material model (Guccione et al., 1991), and the myofiber runs circumferentially at the LV
207 mid wall, the compressive force acting on the initially spherical injections is therefore greatest
208 along the circumferential direction of the LV wall. As a result, the injections were compressed in
209 the circumferential direction of the LV wall. To preserve the injection volumes (as hydrogel is
210 incompressible), the injections became elongated in the transmural direction.

211 Given that the contractive force generated by the myocytes is directly related to the sarcomere
212 length (Guccione et al., 1993; ter Keurs et al., 1980), the decrease in mid-wall sarcomere length
213 (reflected by a decrease in myofiber stretch) should, in principle, decrease the contractive force
214 generated in that region. This effect is apparent in **Figure 3**, which shows a reduced mid-wall
215 ES myofiber stress in RESIDUAL.

216 Another important effect of the injection-induced residual stress is evidenced by the fact that
217 myofiber stretch is much less affected than myofiber stress at ED. This result is possible only if
218 stress components transverse to the fiber direction are changed to balance the change in myofiber
219 stress. Consequently, the myocardium supports a very different state of stress: one with
220 potentially high shear components, and tension in direction normal to the fiber direction (Table
221 1). If cross-fiber sensor located at the Z-disk is indeed present, as suggested by Russell et al.
222 (2010), this difference (in stress state) may also potentially play a critical role in affecting tissue
223 growth.

224 Last, it must be pointed out that the total prescribed injection volume of 0.24 ml is relatively
225 small when compared to other computational models of injection treatment which have larger
226 injection volumes e.g. ~ 5ml (Wall et al., 2006; Wenk et al., 2009) and ~ 9.4ml (Kortsmit et al.,
227 2012). We did not increase the injection volume because doing so would lead to a highly
228 distorted mesh near the injections, which would cause numerical instability. As a result, without
229 the presence of residual stresses (NO-RESIDUAL), the injections have little effects on the global
230 averaged myofiber stress and stretch as seen in Table 1.

231

232 **3.3 Ventricular volume change**

233 The little effect on EDV and ESV in RESIDUAL and NON-RESIDUAL is due to the small
234 amount of injection prescribed in our models as discussed above. In other computational models
235 of injection treatment (Wall et al., 2006; Wenk et al., 2009), a larger injection volume produced
236 a greater effect on EDV and ESV.

237

238 **3.4 Limitations**

239 The key limitation of this model is the assumption of spherical voids that have a radius of 1mm
240 in the myocardium, which of course, is an idealization. The void is most likely not perfectly
241 spherical and uniform in size. Moreover, the inflation of voids during the injection process could
242 be further complicated by any fracture planes the hydrogel could force open during injection. If
243 all these complications are present, the resultant shape of the injection would most likely be
244 different from our model prediction. For example, the injection of Methacrylated Hyaluronic
245 Acid in normal ovine heart was found to be elongated circumferentially in the myofiber direction
246 (Kichula et al., 2013) as opposed to our model's prediction that the injection is elongated in the
247 transmural direction. Since residual stress can only be present if there is a misfit between the
248 injection and the void, the degree of residual stress is sensitive to the void-to-injection size ratio
249 (**Figure 4**) and how the void deforms and expands with injection. Experimental studies providing
250 information on the shape and sizes of the myocardial voids could be performed in the future so
251 that the degree and effects of residual stress can be better quantified.

252

253 **3.5 Summary**

254 In conclusion, we have described the first model that incorporates the effects of residual stress
255 introduced by the injection of materials into the LV. Our results show that the stress and stretch
256 fields near the injection region became more heterogeneous, whereby myofibers between the
257 injections were unloaded and myofibers between the injections and both endocardium and
258 epicardium were pre-stretched. These results are preliminary and models that incorporate more
259 detailed microstructural information are needed to shed light on the possible role of residual
260 stress in the reported therapeutic effects associated with the injection treatment.

261

262 **4. ACKNOWLEDGEMENT**

263 This study was supported by National Heart, Lung, and Blood Institute Grants R01-HL-077921,
264 R01-HL-118627 (to J. M. Guccione), and by a Marie-Curie International Outgoing Fellowship
265 within the 7th European Community Framework Programme (M. Genet). We would like to
266 thank Pamela Derish in Department of Surgery at UCSF for proofing the manuscript

267 **5. REFERENCES**

- 268 Christman, K.L., Fok, H.H., Sievers, R.E., Fang, Q., Lee, R.J., 2004. Fibrin glue alone and
 269 skeletal myoblasts in a fibrin scaffold preserve cardiac function after myocardial infarction.
 270 *Tissue Eng.* 10, 403–9.
- 271 Frank, J.S., Langer, G. a, 1974. The myocardial interstitium: its structure and its role in ionic
 272 exchange. *J. Cell Biol.* 60, 586–601.
- 273 Guccione, J.M., McCulloch, A.D., Waldman, L.K., 1991. Passive material properties of intact
 274 ventricular myocardium determined from a cylindrical model. *J. Biomech. Eng.* 113, 42–55.
- 275 Guccione, J.M., Waldman, L.K., McCulloch, A.D., 1993. Mechanics of active contraction in
 276 cardiac muscle: part II-cylindrical models of the systolic left ventricle. *J. Biomech. Eng.*
 277 115, 82–90.
- 278 Jiang, X.J., Wang, T., Li, X.Y., Wu, D.Q., Zheng, Z. Bin, Zhang, J.F., Chen, J.L., Peng, B.,
 279 Jiang, H., Huang, C., Zhang, X.Z., 2009. Injection of a novel synthetic hydrogel preserves
 280 left ventricle function after myocardial infarction. *J. Biomed. Mater. Res. A* 90, 472–7.
- 281 Kichula, E.T., Wang, H., Dorsey, S.M., Szczesny, S.E., Elliott, D.M., Burdick, J. a, Wenk, J.F.,
 282 2013. Experimental and Computational Investigation of Altered Mechanical Properties in
 283 Myocardium after Hydrogel Injection. *Ann. Biomed. Eng.*
- 284 Kortsmiit, J., Davies, N.H., Miller, R., Macadangdang, J.R., Zilla, P., Franz, T., 2012. The effect
 285 of hydrogel injection on cardiac function and myocardial mechanics in a computational
 286 post-infarction model. *Comput. Methods Biomech. Biomed. Engin.*
- 287 Landa, N., Miller, L., Feinberg, M.S., Holbova, R., Shachar, M., Freeman, I., Cohen, S., Leor, J.,
 288 2008. Effect of injectable alginate implant on cardiac remodeling and function after recent
 289 and old infarcts in rat. *Circulation* 117, 1388–96.
- 290 Lee, L.C., Wall, S.T., Klepach, D., Ge, L., Zhang, Z., Lee, R.J., Hinson, A., Gorman, J.H.,
 291 Gorman, R.C., Guccione, J.M., 2013a. Algisyl-LVR™ with coronary artery bypass grafting
 292 reduces left ventricular wall stress and improves function in the failing human heart. *Int. J.*
 293 *Cardiol.* 168, 2022–2028.
- 294 Lee, L.C., Zhihong, Z., Hinson, A., Guccione, J.M., 2013b. Reduction in left ventricular wall
 295 stress and improvement in function in failing hearts using Algisyl-LVR. *J. Vis. Exp.* 1–6.
- 296 Nelson, D.M., Ma, Z., Fujimoto, K.L., Hashizume, R., Wagner, W.R., 2011. Intra-myocardial
 297 biomaterial injection therapy in the treatment of heart failure: Materials, outcomes and
 298 challenges. *Acta Biomater.* 7, 1–15.

299 Russell, B., Curtis, M.W., Koshman, Y.E., Samarel, A.M., 2010. Mechanical stress-induced
300 sarcomere assembly for cardiac muscle growth in length and width. *J. Mol. Cell. Cardiol.*
301 48, 817–23.

302 Streeter, D.D., Spotnitz, H.M., Patel, D.P., Ross, J., Sonnenblick, E.H., 1969. Fiber orientation in
303 the canine left ventricle during diastole and systole. *Circ. Res.* 24, 339–47.

304 Sun, K., Stander, N., Jhun, C.S., Zhang, Z., Suzuki, T., Wang, G.Y., Saeed, M., Wallace, A.W.,
305 Tseng, E.E., Baker, A.J., Saloner, D., Einstein, D.R., Ratcliffe, M.B., Guccione, J.M., 2009.
306 A computationally efficient formal optimization of regional myocardial contractility in a
307 sheep with left ventricular aneurysm. *J. Biomech. Eng.* 131, 111001.

308 Ter Keurs, H.E., Rijnsburger, W.H., van Heuningen, R., Nagelsmit, M.J., 1980. Tension
309 development and sarcomere length in rat cardiac trabeculae. Evidence of length-dependent
310 activation. *Circ. Res.* 46, 703–714.

311 Wall, S.T., Walker, J.C., Healy, K.E., Ratcliffe, M.B., Guccione, J.M., 2006. Theoretical impact
312 of the injection of material into the myocardium: a finite element model simulation.
313 *Circulation* 114, 2627–35.

314 Wenk, J.F., Klepach, D., Lee, L.C., Zhang, Z., Ge, L., Tseng, E.E., Martin, A., Kozerke, S.,
315 Gorman, J.H., Gorman, R.C., Guccione, J.M., 2012. First evidence of depressed
316 contractility in the border zone of a human myocardial infarction. *Ann. Thorac. Surg.* 93,
317 1188–93.

318 Wenk, J.F., Wall, S.T., Peterson, R.C., Helgerson, S.L., Sabbah, H.N., Burger, M., Stander, N.,
319 Ratcliffe, M.B., Guccione, J.M., 2009. A method for automatically optimizing medical
320 devices for treating heart failure: designing polymeric injection patterns. *J. Biomech. Eng.*
321 131, 121011.

322

323

324

325

326

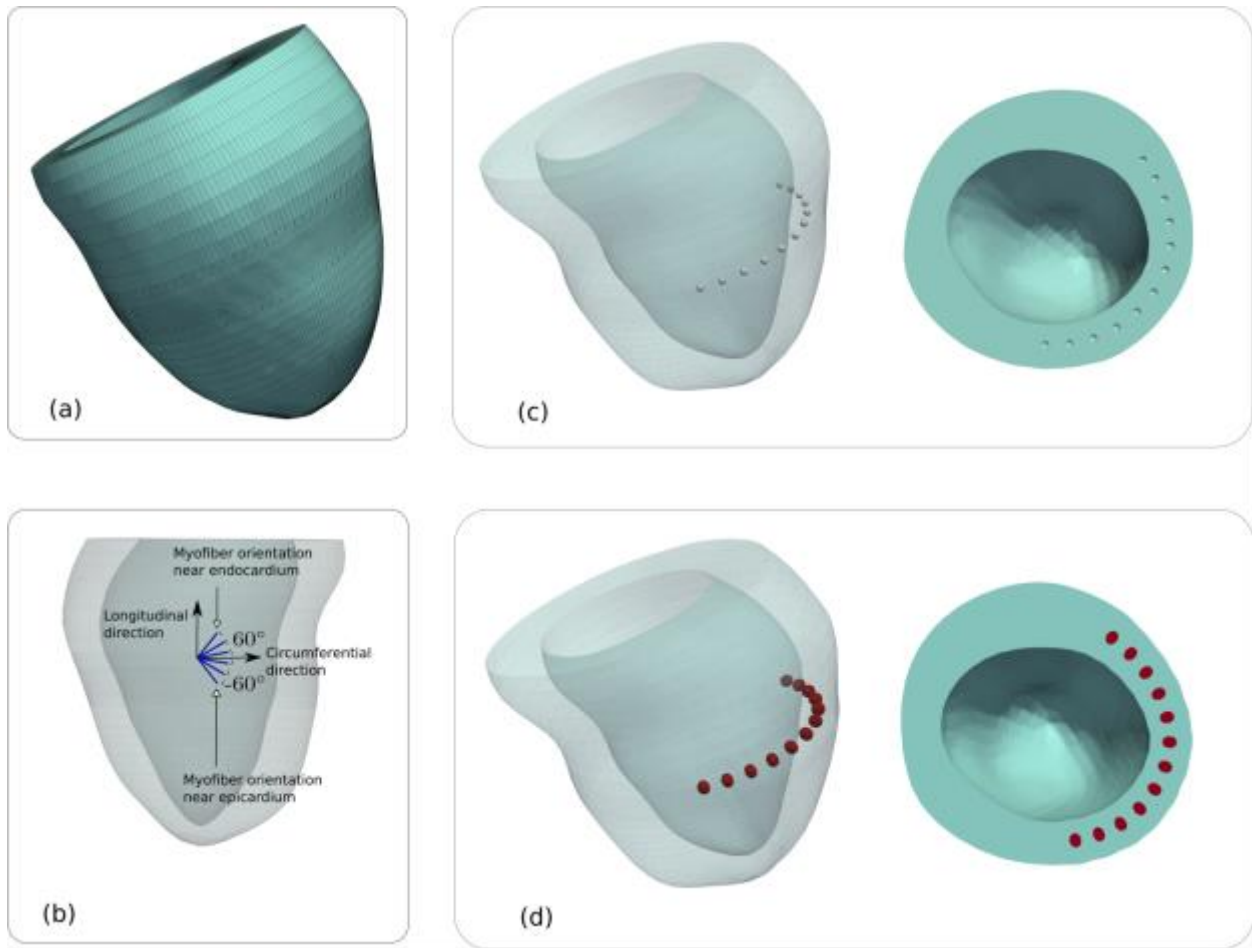
327

328 **6. TABLES**

329 **Table 1:** Myofiber and cross-myofiber stretch and stress (average \pm standard deviation at end-
 330 diastole (ED) and end-systole (ES). Refer to text description of BASELINE, RESIDUAL and
 331 NO-RESIDUAL.

		BASELINE	RESIDUAL	NO-RESIDUAL
Myofiber stretch	ED	1.12 \pm 0.02	1.11 \pm 0.04	1.12 \pm 0.02
	ES	0.97 \pm 0.03	0.97 \pm 0.04	0.97 \pm 0.03
Cross Myofiber stretch	ED	1.12 \pm 0.05	1.11 \pm 0.06	1.12 \pm 0.04
	ES	1.00 \pm 0.06	1.01 \pm 0.07	1.01 \pm 0.07
Myofiber stress (kPa)	ED	6.9 \pm 4.6	11.2 \pm 48.8	6.7 \pm 4.6
	ES	30 \pm 15	35.1 \pm 50.9	30 \pm 15
Cross Myofiber stress (kPa)	ED	3.9 \pm 3.8	8.1 \pm 50.1	3.8 \pm 3.8
	ES	8.1 \pm 8.2	13.4 \pm 57.9	8.1 \pm 8.3

332 **7. FIGURES**



333

334 **Figure 1**(a): Finite element mesh of the patient-specific LV. (b): Transmurality of the myofiber orientation.
 335 Left ventricular mesh with (c): 12 spherical voids each having a 1mm radius and (d): injections (red) filling up the
 336 void spaces. Notice that the injections are no longer spherical and are slightly elongated transmurally.

337

338

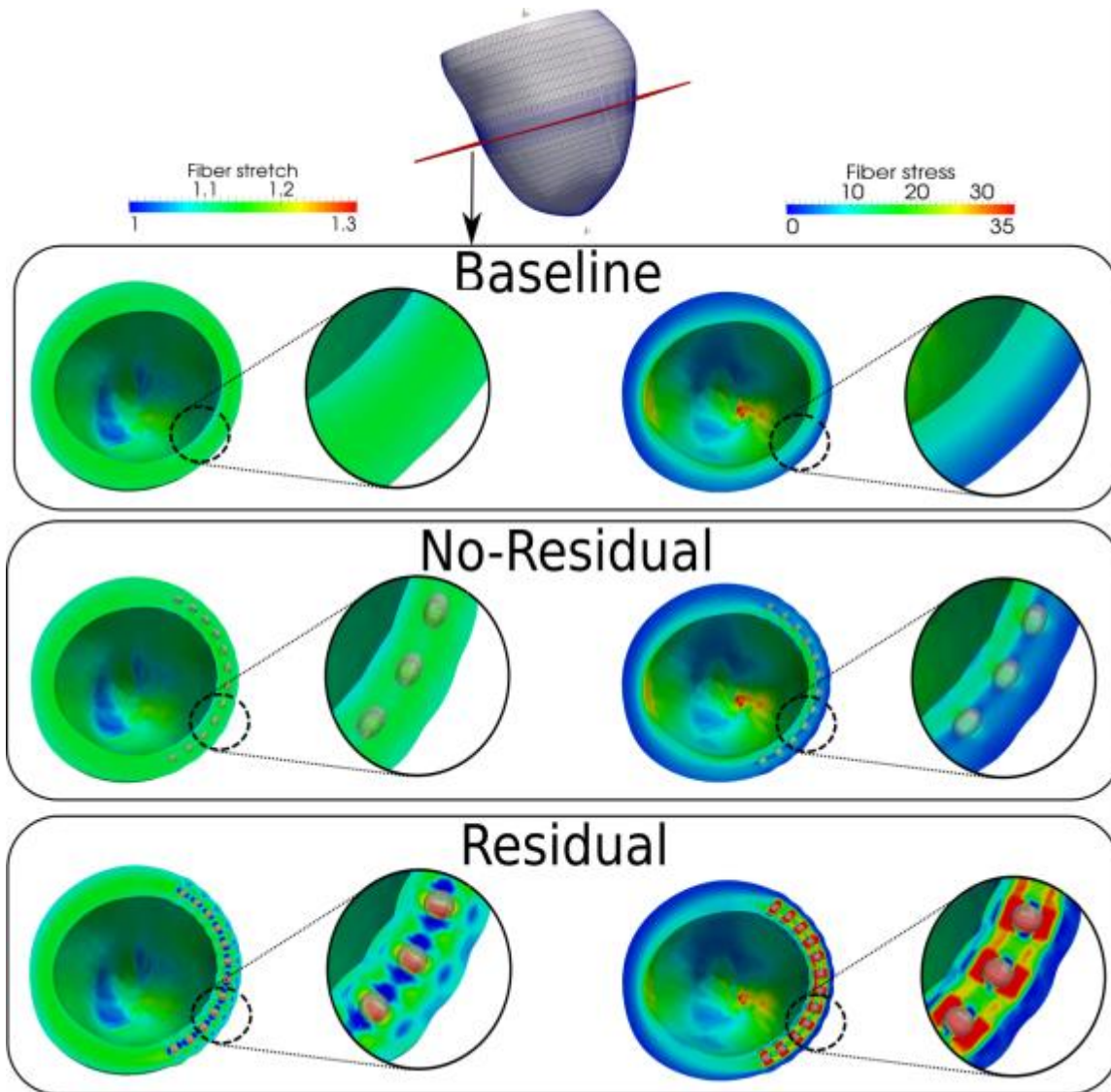
339

340

341

342

343

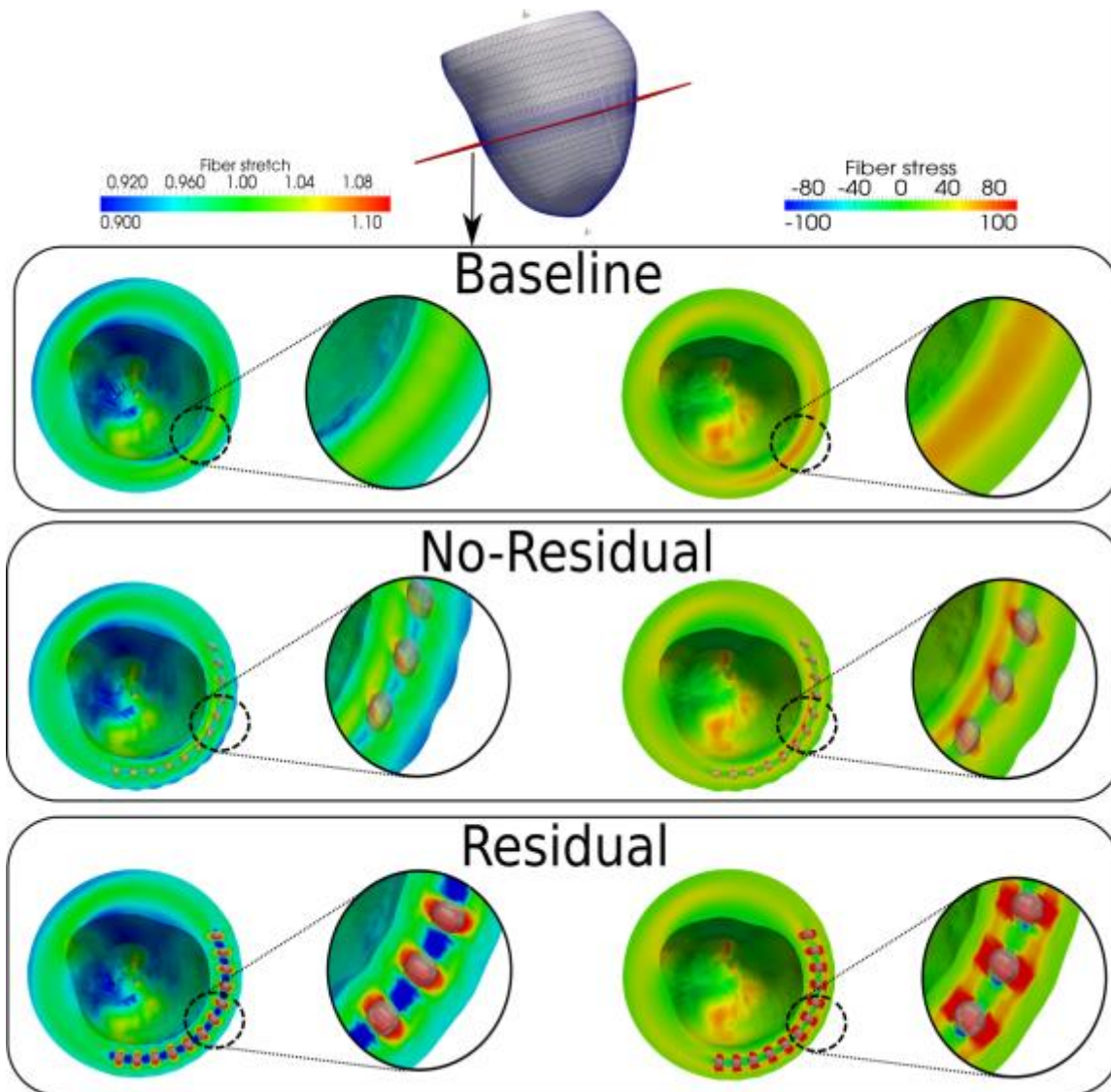


344

345 **Figure 2:** Comparison of fiber stretch and stress for the baseline, no-residual and residual cases at end-of-diastole.

346 Cutting plane is shown in red at the top picture. Unit of fiber stress is kPa.

347



348

349 **Figure 3:** Comparison of fiber stretch and stress for the baseline, no-residual and residual cases at end-of-systole
 350 Cutting plane is shown in red at the top picture. Arrow in the residual case indicates the reduced midwall end-
 351 systolic myofiber stress. Unit of fiber stress is kPa.

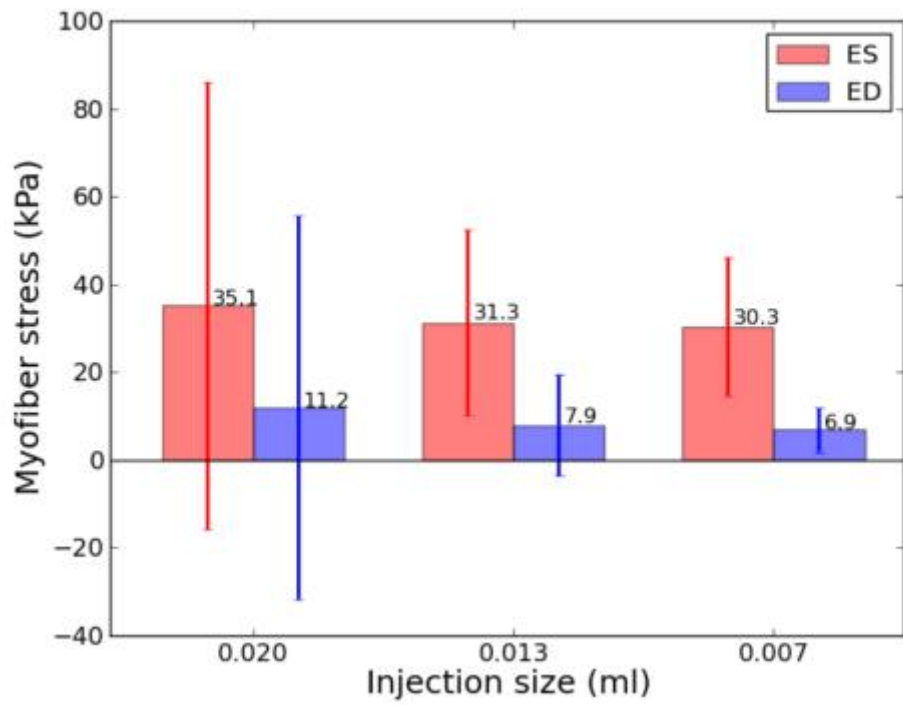
352

353

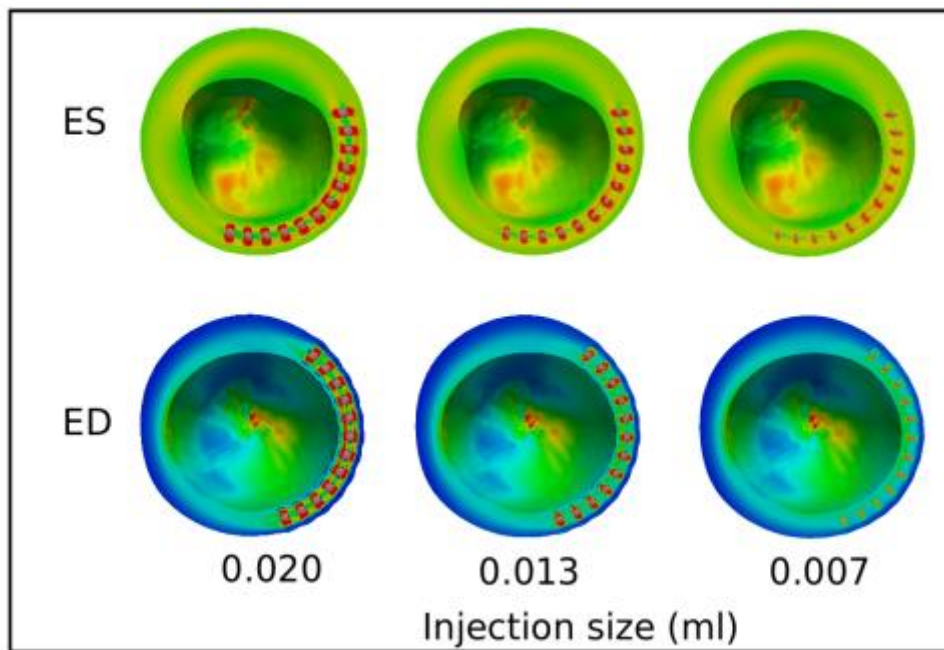
354

355

356



(a)



(b)

357

358 **Figure 4:** Effects of injection size (with constant void size) on (a) global myofiber stress and (b) regional myofiber
 359 stress near the injection sites. Mean values of myofiber stress are given on top of each bar in (a). Refer to Fig. 2 and
 360 3's legend for ED and ES regional myofiber stress in (b), respectively.